D6

S.E. Woosley
Editor

Supernovae

The Tenth Santa Cruz Workshop
in Astronomy and Astrophysics
July 9 to 21, 1989, Lick Observatory

With 311 Illustrations

Springer-Verlag
New York Berlin Heidelberg London
Paris Tokyo Hong Kong Barcelona

BIBLIOGRAPHY

Berger, M. J., and Colella, P., 1989, to appear in J. Comp. Phys.

Braun, R. and Strom, R.G., 1986, Astronomy and Astrophysics 164, 193.

Braun, R., 1988, IAU Coll. 101, Supernova Remnants and the Interstellar Medium, Ed. R. S. Roger and I. L. Landecker, Cambridge Univ. Press, 227.

Chevalier, R. A., 1976, Ap.J., 207, 450.

Colella, P. and Woodward, P., 1984, J. Comp. Phys. 54, 174.

Glaz, H. M., Colella, P., Glass, I.I., Deschambault, R. L., 1985, Proc. Roy. Soc. Lond. A 398, 117.

Hornung, H., 1986, Ann. Rev. Fluid Mech., 18, 33.

Klein, R. I., Colella, P. and McKee, C. F., 1989, Ap. J. in preparation.

Klein, R. I., Colella, P., and McKee, C. F., 1989a, "The Physics of Compressible Turbulent Mixing International Workshop", Princeton University, Ed. W. Dannevik, 1989, Springer Verlag, New York Inc., Lecture Notes Series.

Klein, R. I., McKee, C. F. and Colella, P., Proceedings of the Astronomical Society of the Pacific, 100th Centennial, Berkeley, Calif., Ed. L. Blitz, 1989b.

McKee, C. F. and Cowie, L. L., 1975, Ap.J., 195, 715.

McKee, C. F., 1988, IAU Coll.101, Supernova Remnants and the Interstellar Medium, Ed. R. S. Roger and I. L. Landecker, Cambridge Univ. Press, 205.

Nulsen, P.E.J. 1982, M.N.R.A.S., 198, 1007.

Richtmyer, R.D., 1960, Comm. Pur. Appl. Math., 13, 297.

Saffman P. G., Baker, G. R., 1979, Ann. Rev. of Fluid Mech. 11, 95.

Spitzer, L., 1982, Ap.J., 262, 315.

Tuff, R. J., 1986, M.N.R.A.S., 219, 13.

Velusamy, T., 1988, IAU Coll 101, Supernova Remnants and the Interstellar Medium, Ed. R. S. Roger and I. L. Landecker, Cambridge Univ. Press, 265.

The Effect of Supernova Remnants on Interstellar Clouds

Richard I. Klein, Christopher F. McKee, & Philip Colella

INTRODUCTION

The interaction between supernova remnants (SNRs) and interstellar clouds in the galaxy is known to play a major role in determining the structure of the interstellar medium (ISM). We know that the ISM is highly inhomogeneous, consisting of both diffuse atomic clouds (T~100K) and dense molecular clouds (T~10K) surrounded by a low density warm ionized gas (T~10^4K) and by a very hot coronal gas (T~10^6K). Next to radiation directly from stars, supernova explosions represent the most important form of energy injection into the ISM; they determine the velocity of interstellar clouds, accelerate cosmic rays, and can compress clouds to gravitational instability, possibly spawning a new generation of star formation. The shock waves from supernova remnants can compress, accelerate, disrupt and render hydrodynamically unstable interstellar clouds, thereby ejecting mass back into the intercloud medium. Thus, while the interaction of the SNR blast wave with cloud inhomogeneities can clearly alter the appearance of the ISM, the cloud inhomogeneities can similarly have a profound effect on the structure of the SNR.

Recent observations of SNR of enhanced emission in the Balmer line filaments show evidence of cloud shock interactions for Tycho (Braun, 1988). Velusamy (1987) finds evidence of the remnant cloud interaction in his radio observations of W28 and W44 taken at 327 MHz. These observations clearly show the distortion of the radio shell as the remnant begins to wrap around a dense cloud. The observations of the SNR IC443 by Braun and Strom (1986) show the later evolution of the cloud shock interacting with the outer layers of the cloud stripped off at high velocity.

Given the importance of the interaction of the supernova shocks with clouds for understanding the structure and the dynamics of the ISM as well as the potential importance of the interaction as a means of triggering new star formation, the problem has been studied both analytically and numerically over the past decade. All of the previous work on this important problem leave unanswered several questions of key importance: What is the ultimate fate of clouds that have been impacted by SNR shocks? What is the total momentum delivered to the cloud? How much mass is lost from the cloud? What are the mechanisms by which clouds are disrupted and to what extend does disruption take place? How does cloud morphology scale with cloud density, shock Mach number and cloud size? Is the cloud driven to gravitational instability or is the cloud destroyed? What is the effect of the interstellar magnetic field on the evolution? What are the observable consequences of the interaction?

We have recently found (Klein, Colella and McKee, 1989a,b) that highly complex shock-shock interactions and instabilities and shear flow motions play a major role in determining the morphology of the cloud. To address these physical complexities, we have used the local adaptive mesh refinement techniques with second order Godonov methods for 2-D axisymmetry developed by Berger and Colella, 1989 (cf. Klein, Colella, and McKee, 1989a,b). We assume that the cloud and intercloud gas are both adiabatic, although we allow the cloud and intercloud medium to have different values of the adiabatic index γ.

From the point of view of being able to resolve detailed complex physical structures with reasonable amounts of supercomputer time and memory, the most important feature of our code is that it employs a dynamic regridding strategy known as local Adaptive Mesh Refinement (AMR) to dynamically refine the solution in regions of interest or excessive error.

This is effected by placing a finer grid over the region in question with the grid spacing reduced by some even factor (typically) in each spatial dimension. Multiple levels of grid refinement are possible with the maximum number of nested grids supplied as a parameter in the calculation. Typically our calculations employ two nested grids over the initial coarse grid.

CLOUD SIZE SCALES

As the SNR expands through the ISM, it drives a shock into any cloud it encounters. Assuming that these are strong shocks, the pressure behind the blast wave and the pressure behind the transmitted cloud shock are comparable, and one finds that (McKee and Cowie, 1975)

$$v_s = (\rho_i/\rho_c)^{1/2} v_b \, , \tag{1}$$

where v_s and v_b are the cloud shock and blast wave velocities and ρ_c and ρ_i the initial cloud and intercloud densities, respectively. Following McKee (1988), we define characteristic timescales for the cloud-shock interaction. Let $\chi \equiv \rho_c/\rho_i$ be the density contrast and assume that $\chi >> 1$. Assume that the cloud is a sphere with radius a at a distance R_b from the supernova explosion. The blast wave in the Sedov-Taylor phase will expand as $R_b \propto t^{2/5}$, so the age of the SNR is,

$$t \equiv \frac{dR_b}{dt} = \frac{2}{5}\frac{R_b}{v_b} \, . \tag{2}$$

The blast wave in the intercloud medium crosses the cloud in a time

$$t_{ic} \equiv \frac{2a}{v_b} \, , \tag{3}$$

whereas the cloud shock crushes the cloud in a time

$$t_{cc} \equiv \frac{a}{v_s} = \frac{\chi^{1/2} a}{v_b} \, . \tag{4}$$

The cloud crushing time t_{cc} is of the order of the sound crossing time in the crushed cloud; it is also about the timescale for the growth of large scale Rayleigh-Taylor instabilities. Finally, the cloud accelerates up to the velocity of the intercloud gas in a characteristic drag time t_d defined by $\rho_i v_b t_d = \rho_c a$, or

$$t_d = \frac{\chi a}{v_b} = \chi^{1/2} t_{cc} \, . \tag{5}$$

In this paper, we will consider only clouds that can be characterized as "small", so that the SNR does not evolve significantly during the time for the cloud to be crushed:

$$t > t_{cc} \Rightarrow a < \frac{0.4R}{\chi^{1/2}} \, . \tag{6}$$

Indeed, we shall focus on the case in which the cloud is "very small", so that $t >> t_d$, and $a << 0.4R/\chi$. In either case, we have $a << R$ so that the blast wave may be treated as a planar shock. In the opposite limit of a shock interaction with a large cloud, the SNR blast wave will undergo substantial weakening over the time it takes to cross the cloud. We expect substantial disruption for the small clouds, but only impulsive effects for large clouds.

CLOUD EVOLUTION

a. Cloud Crushing

Since there are no intrinsic scales in the problem, it is parameterized by the Mach number of the SNR blast wave M and the density ratio χ. Our calculations assumed 2-D axisymmetry for an inviscid fluid with no magnetic field. Two cases were considered for the cloud: $\gamma=1.1$ and $\gamma=5/3$. The intercloud gas was assumed to have $\gamma=5/3$. Several calculations have been made for Mach numbers in the range 10-1000 and density ratios 10-400.

It is useful to follow the morphological evolution of the cloud through several cloud crushing times to obtain a sense of the different stages of development. We present the time-development of the isodensity contours of the cloud for the case γ (cloud) = γ (intercloud) = 5/3, $\chi=10$, $M=10$. At $t=0.84\ t_{cc}$ (Fig. 1), the transmitted shock is compressing the cloud from the front, secondary shocks have enveloped the sides of the cloud as the blast wave passes over the cloud, and a reflected bow shock moves upstream into the intercloud medium. The reflected shock becomes a standing bow shock and eventually a weak acoustic wave carrying away a small amount of energy from the supernova shock (Spitzer, 1982). At $t=1.05t_{cc}$ (Fig. 2) the blast wave behind the cloud reflects off the axis giving rise to a Mach reflected shock back into the cloud. Substantial flattening of the cloud is observed at $t=2.1t_{cc}$ from the strong shocks which have squeezed it like a vise. The pressure maximum on the nose of the cloud exceeds the pressure minimum on the sides and the cloud begins to expand laterally (Fig. 3). We note the growth of Richtmyer-Meshkov instabilities (Richtmyer, 1960) on the cloud nose which grow more slowly than the classic Rayleigh Taylor modes and evidence of Kelvin Helmholtz instabilities on the sides of the cloud.

b. Shear Flow and Vortex Production

At $3.78t_{cc}$ a prominent shear layer exists due to the motion of the cloud through the ICM. The shear produces copious vortex rings along the shear flow layer. The cloud consists of a distorted unstable axially flattened core component and a severely disrupted halo of cloud material. Over 70% of the original cloud mass is in small fragments which, in the absence of cooling, should merge with the intercloud medium. The unstable break up is dominated by large scale differential shear. At $t=9.7\ t_{cc}$, the cloud is completly destroyed (Fig. 4) and consists of several thousand fragments. At $4.2\ t_{cc}$ the strong supersonic vortex rings align along the shear flow layer produced in the dominant arm of cloud material that has been pulled from the main core of the cloud as well as along a second substantially fractured mass of cloud that has been fragmented from the arm. In Fig. 5 we show the associated flow field alongside of isodensity contours of the cloud and intercloud gas at $t=4.2\ t_{cc}$. It is clear that regions of strong circulation (high vorticity, numbered 1-5) are associated with positions along the shear flow layer where the cloud has undergone severe fragmentation. As vortex rings are formed in the shear layer and move away from the initial cloud are, the vortex rings are broken off. The process is called vortex shedding. It is suggestive of the possibility that the vorticity in the intercloud matter is acting to enhance the cloud break-up along the differential shear layer, thus acting as a mix-master aiding the development of the Kelvin-Helmholtz instabilities. This interesting possibility is worth further study.

The vorticity depends upon a baroclinic term which is the major source of vorticity in the cloud-shock interaction. The shock is curved as it interacts with the cloud surface and produces surfaces of constant pressure that are not coincident with surfaces of constant density at the interface of the cloud and intercloud matter. This gives a non-zero cross product of gradients. The vorticity in the ICM is greater than that in the cloud because of the higher velocities in the lower density material. Our calculations show that most of the vorticity remains concentrated near the cloud boundary, where it originated. An additional term that can be important is vortex diffusion. If the gas has a frictional force due to viscosity, F/ρ, it can be represented as $F/\rho = \nu\nabla^2 u$ where ν is the viscosity; then $\nabla x(F/\rho) \sim \nu\nabla^2\omega$. This represents the diffusion of vorticity from regions of high to low concentration. It is proportional to the amount of numerical viscosity in the finite difference approximations. Given the importance of vorticity as a possible observational diagnostic of the remnant cloud

·rized by the Mach number of
ıs assumed 2-D axisymmetry
re considered for the cloud:
γ = 5/3. Several calculations
nsity ratios 10-400.

cloud through several cloud
›pment. We present the time-
e γ (cloud) = γ (intercloud) =
ck is compressing the cloud
the cloud as the blast wave
pstream into the intercloud
ıd eventually a weak acoustic
va shock (Spitzer, 1982). At
ıe axis giving rise to a Mach
cloud is observed at $t=2.1t_{cc}$
e pressure maximum on the
d the cloud begins to expand
stabilities (Richtmyer, 1960)
Rayleigh Taylor modes and
ıd.

the cloud through the ICM.
yer. The cloud consists of a
rely disrupted halo of cloud
ents which, in the absence of
le break up is dominated by
ietly destroyed (Fig. 4) and
ıpersonic vortex rings align
loud material that has been
substantially fractured mass
ow the associated flow field
, at $t=4.2\ t_{cc}$. It is clear that
e associated with positions
e fragmentation. As vortex
ıl cloud are, the vortex rings
estive of the possibility that
· cloud break-up along the
; the development of the
th further study.
major source of vorticity in
with the cloud surface and
: with surfaces of constant
his gives a non-zero cross
t in the cloud because of the
ons show that most of the
t originated. An additional
s a frictional force due to
the viscosity; then ∇x(F/ρ)
f high to low concentration.
difference approximations.
ostic of the remnant cloud

Density, $t=0.84t_{cc}$

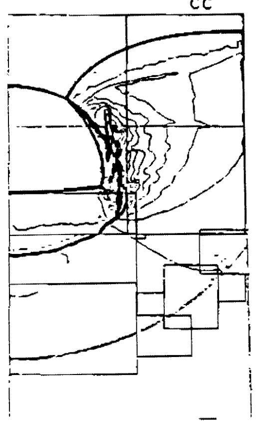

Figure 1

Density, $t=1.05t_{cc}$

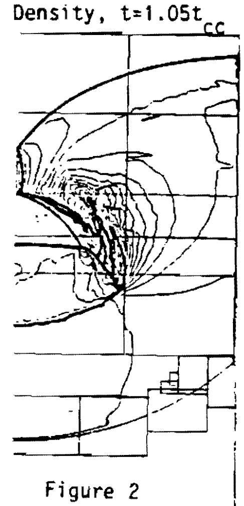

Figure 2

Density, $t=2.1t_{cc}$

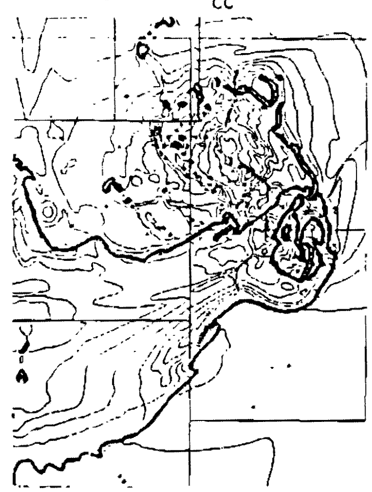

Figure 3

Density, $t=9.7t_{cc}$

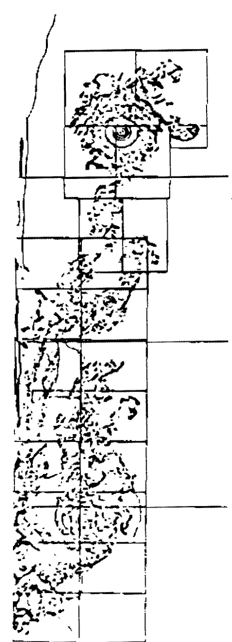

Figure 4

Figures 1-4 Isodensity contours of cloud and intercloud matter at different times.

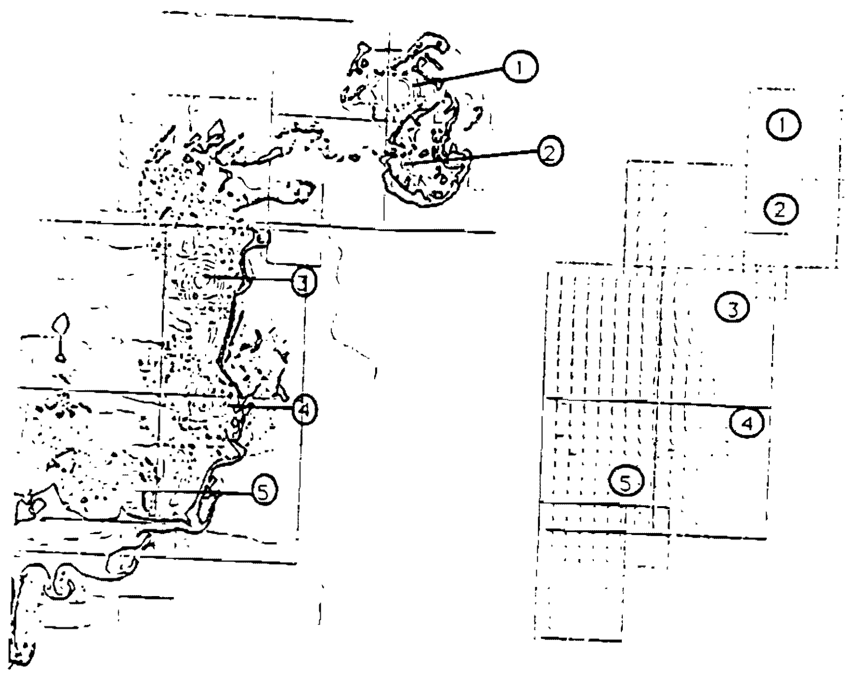

Figure 5 Isodensity contours (on left) at $t=4.2\ t_{cc}$, flow field (on right). Numbers are sites of vorticity maximums.

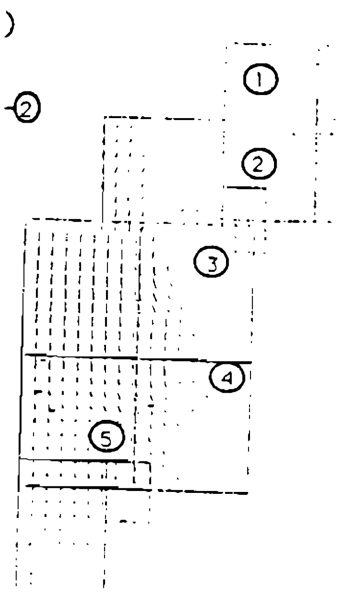

t_{cc}, flow field (on right).
s.

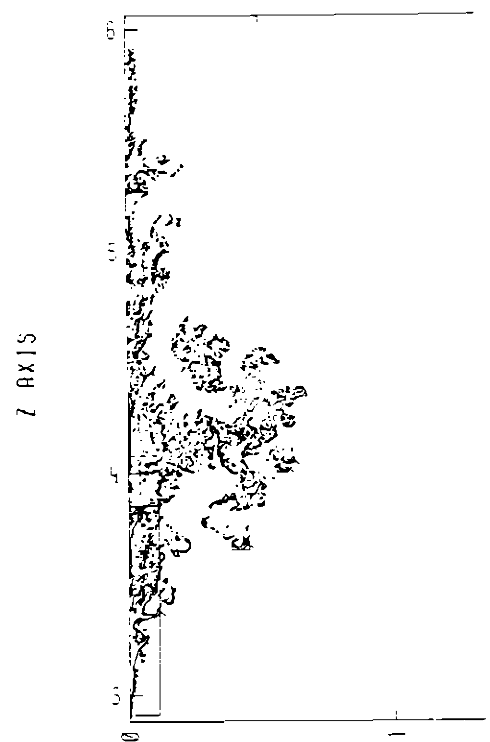

Figure 6 Isodensity contours for χ=100, M=100 at t=4.0 t_{cc}

interaction as well as its possible role in the cloud fragmentation, it is of great importance to demonstrate that numerical viscosity does not play a role in determining the amount of vorticity production. We have computed the time evolution of the cloud for four increasingly resolved initial grids, doubling the number of cells in both Δr and Δz with each increase in resolution. We have found that the time evolution of the vorticity for even the coarsest mesh tracks to a remarkable degree of accuracy the vorticity of the finest grid resolution, which is equivalent to a 7×10^6 zone calculation for a fixed grid method. This clearly establishes that numerical viscosity, which is proportional to grid resolution, does not affect the production of vorticity for the adaptive grid techniques we are using. This type of calculation is a powerful check on the conservation of vorticity.

Let us consider the characterization of the evolution of the interstellar cloud in more detail. In Table 1, we display the results of adiabatic calculations for three models in which $\gamma = 5/3$ in both the cloud and ICM. The calculations are done for two models (M=10 and 100) for density contrast χ =10 and one model (M=100) for density contrast 100. The first entry in the table is the time normalized to the intercloud crossing time. The second entry gives the time normalized to the cloud crushing time and the drag time, $t_d = \chi^{1/2}\, t_{cc}$. The next column is the sound speed behind the cloud shock normalized to the blast wave velocity. The shocked intercloud gas moves at a velocity (3/4) v_b relative to the cloud for $\gamma = 5/3$, so the next entry measures the ratio of the current cloud/intercloud relative velocity Δv to its initial value; in the frame of the shocked intercloud gas, this is a measure of cloud deceleration. The next column is a characterization of the cloud's aspect ratio in the radial and axial direction weighted by its half mass distribution. Here $r_{1/2}$ is the radial half-mass distance and $Z_{1/2}$ is the axial half-mass distance. The last column gives the radial $\dot{r}_{1/2}$ and axial $\dot{Z}_{1/2}$ expansion velocities of the cloud. These velocities are computed by using the half mass distance distributions at the two final times in the calculation.

Table 1

	t/t_{ic}	t/t_{cc} t/t_{drag}	c_c/v_b	$\frac{4}{3}(\Delta v / v_b)$	$r_{1/2}(t)/r_{1/2}(0)$ $Z_{1/2}(t)/Z_{1/2}(0)$	$\dot{r}_{1/2}/v_b$ $\dot{Z}_{1/2}/v_b$
χ=10						
M=10	6.7	4.2 1.3	0.18	0.16	1.8 3.2	~0.0 0.35
	15.3	9.66 3.0		0.074	2.38 5.69	~0.0 ≤0.045
M=100	6.7	4.2 1.3	0.18	0.14	2.0 2.6	~0.0 0.32
χ=100						
M=100	21.3	4.3 0.43	.056	0.25	3.7 8.4	~0.0 0.42

Several conclusions can be drawn from these results. Comparing the results at the same normalized "final" time $t = 4.2t_{cc}$ for clouds of the same density $\chi = 10$, but subjected to blast waves of different Mach number, 10 and 100, we note that both clouds have decelerated to about 0.15 of their initial velocities. Thus, these clouds have almost stopped, leading to a small pressure differential between the front of the cloud surface and the sides so that there is

ation, it is of great importance to
· in determining the amount of
of the cloud for four increasingly
Δr and Δz with each increase in
ticity for even the coarsest mesh
e finest grid resolution, which is
od. This clearly establishes that
does not affect the production of
type of calculation is a powerful

· interstellar cloud in more detail.
or three models in which $\gamma = 5/3$
wo models (M=10 and 100) for
contrast 100. The first entry in
me. The second entry gives the
e, $t_d = \chi^{1/2} t_{cc}$. The next column
· the blast wave velocity. The
e to the cloud for $\gamma = 5/3$, so the
relative velocity Δv to its initial
asure of cloud deceleration. The
in the radial and axial direction
l half-mass distance and $Z_{1/2}$ is
al $\dot{r}_{1/2}$ and axial $\dot{Z}_{1/2}$ expansion
y using the half mass distance

2(0)	$\dot{r}_{1/2}/v_b$
1/2(0)	$\dot{Z}_{1/2}/v_b$
	~0.0
	0.35
	~0.0
	≤0.045
	~0.0
	0.32
	~0.0
	0.42

nparing the results at the same
ity χ = 10, but subjected to blast
both clouds have decelerated to
ve almost stopped, leading to a
ace and the sides so that there is

little force driving further radial expansion; hence the clouds have a radial expansion velocity $\dot{r}_{1/2} = 0$. The strong shear flow in the cloud is still dominant, however, and both clouds are supersonically shearing apart at about the same axial expansion velocity $\dot{Z}_{1/2}$ of 3 times the cloud velocity. The physical extent of the stretching in both the radial and axial direction

$$\frac{r_{1/2}(t)}{r_{1/2}(0)}, \frac{Z_{1/2}(t)}{Z_{1/2}(0)}$$

is essentially the same for the two cases. The remarkable agreement of these features of the clouds and their similar morphological structure leads one to suspect that the cloud evolution may scale similarly with the Mach number of the SNR shock. This Mach scaling can be clearly seen if we scale the time, velocity and pressure as $t' = t/M$, $v' = vM$ and $P' = PM$. Substituting these scaled quantities into the Euler equations, we find that Euler equations are invariant under this transformation. Thus, we find that for fixed γ and density contrast χ, the morphological evolution is a function of t/t_{cc} only, in the limit of large M.

Clouds with greater density contrasts χ show greater expansion in both the radial and axial directions, as shown both by the results in Table 1 and by Fig. 6, which portrays the state of a shocked cloud with χ = 100 at 4 t_{cc}. This follows from the fact that the characteristic expansion time for the cloud is the sound crossing time (which, as remarked above, is about t_{cc}), whereas the time for the cloud to decelerate is the drag time $t_d = \chi^{1/2} t_{cc}$. The lateral expansion of the cloud is due to the lower pressure on the sides of the cloud caused by the Venturi effect (Nittman et al. 1982). This pressure difference decays on the drag time; by the time shown in Fig. 6, this expansion has stopped. At $t = 4\ t_{cc}$, the axial expansion velocity is a substantial fraction of v_b for both χ = 10 and χ = 100; since t_{cc} is larger for χ = 100, the length of the cloud is greater in this case. We expect the axial expansion of the cloud to stop within a few drag times. This has been verified for the χ = 10 case, but not the χ = 100 case.

c. Cloud Fragmentation

At late times (several t_{cc}) the clouds is turbulent with many fragments reduced to a foam on the scale of grid resolution. It is of great interest to follow the mass loss of the cloud as it fragments, and to understand how the fragmentation scales with varying cloud density. In Fig. 7, we show the mass of the cloud core as a function of time for clouds with density contrasts χ=10,100,400. The cloud core is defined to be the most massive cloud fragment. The mass loss vs time has been fitted with a exponential to determine the fragmentation time t_f, defined as the time for each cloud to be left with 1/e of its original mass. We find for χ=10 that the cloud fragments initially into two roughly equal mass fragments. The mass fragments then begin a series of further fragmentation stages into smaller pieces due to combined Rayleigh Taylor and Kelvin Helmholtz instabilities. In Fig. 4 we show isodensity contours of the cloud at t=9.67 t_{cc} where the cloud is completely destroyed. The final fate of this cloud consists of a quasi-static halo of fragments of which 50% of the mass resides in an axially elongated distribution stretched out 5-6 times its initial shape, and the rest of the mass resides in a multitude of fragments much less dispersed.

For clouds with χ>>10, the stripping process proceeds differently. For χ=400, the cloud fragments gradually, with a continuous erosion by loss of small fragments (cf. Fig. 7, Fig. 8). Since small fragments rapidly become comoving with the intercloud medium whereas the cloud core decelerates gradually, small fragments trail far behind the massive cloud core until the core itself is destroyed by Kelvin-Helmholtz instabilities as it drags through the intercloud medium. The cloud core mass at $t = 2t_{cc}$ (Fig. 8) is 26% of the original cloud and we see that the cloud has the distinct morphology of a dense cloud core trailed by a multitude of fragments in a narrow tail.

Our results show that clouds are fragmented in a time $t_f \sim (1.5 - 4)\ t_{cc}$ as χ ranges from 400 to 10; recall that t_{cc} is of order the Rayleigh Taylor timescale. The numerical coefficient is smaller for the higher density contrasts, presumably because the relative velocity of the cloud remains greater.

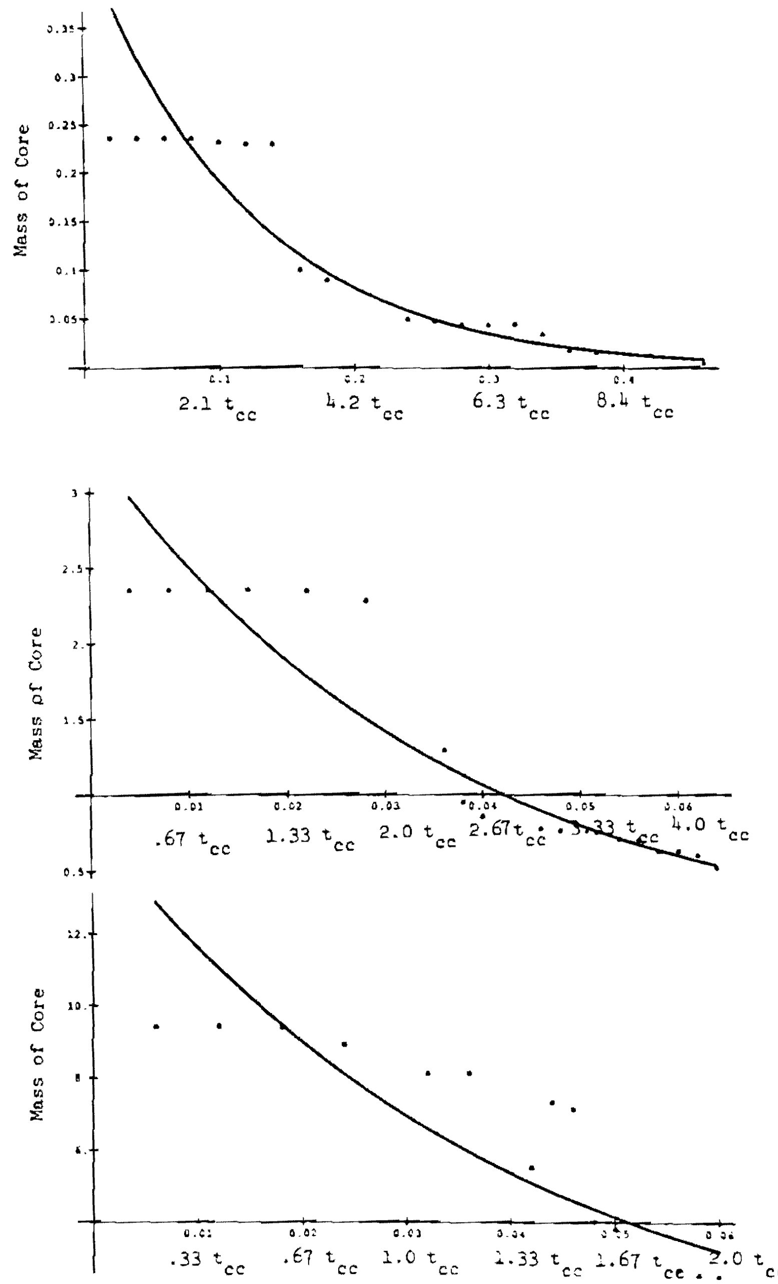

Figure 7 Core mass vs time for χ=10, 100, 400

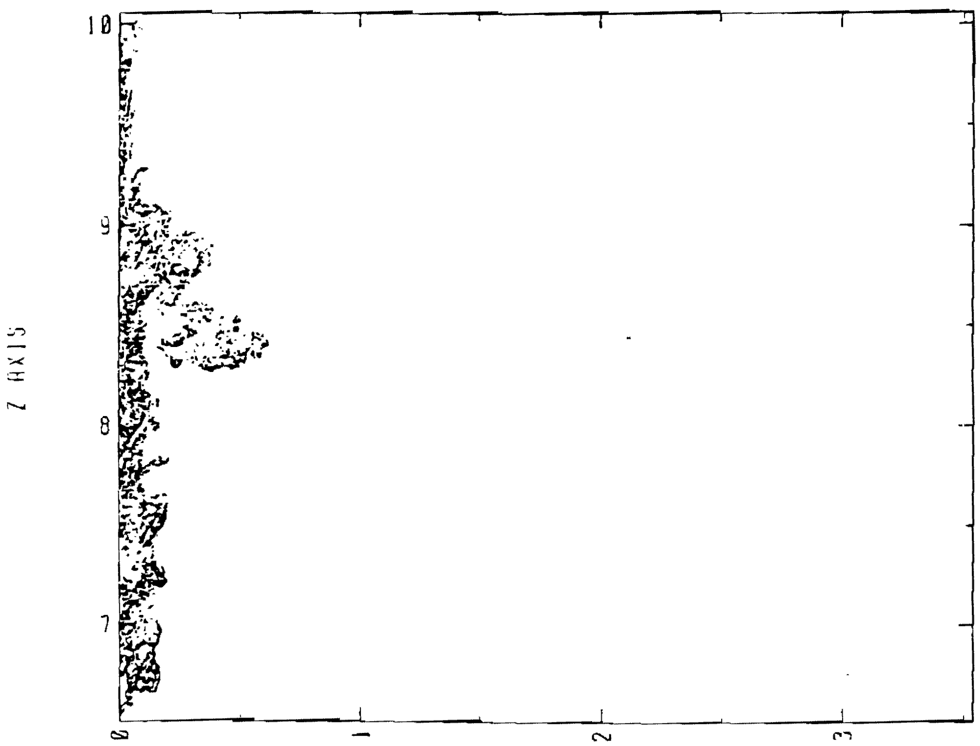

Figure 8 Isodensity contours for χ=400, M=100 at t=2.0 t_{cc}. Note morphology of cloud consisting of a dense "head" followed by a trail of several thousand fragments with an aspect ratio of 20 to 1.